Flexural and Dynamic Characteristics of FRP Composite Sandwich Beam

Shah Alam
Department of Mechanical Engineering,
Texas A&M University, Kingsville, TX 78363,
USA

Guoqiang Li
Department of Mechanical Engineering,
Louisiana State University, Baton Rouge,
LA 70803

Abstract— **This study presents the flexural and impact testing results of composite sandwich beams. The sandwich beams are constructed from balsa wood in the core and high strength steel wire and E-glass fiber reinforced polymer composite in the facings. The testing of these beams is performed using a monotonic static three-point loading to failure in accordance with ASTM standard C393-00. Local strain distribution in the mid-span of the beams is obtained using strain gauges. Mid-span deflections of the beams are real-time measured using linear variable displacement transducer (LVDT). From the experimental results, flexural properties of the beams are calculated, including bending stiffness, bending strength, shear strength etc. The experimental results have shown that the beams have all failed in the compression zone local buckling of the top face and shear of the core. The bottom skin does not exhibit any type of premature failure or distress. No bond failure of the composite in the tension zone is observed in any of the tested beams. After the bending tests, the overhanging portion of the sandwich beams are machined into various scaled-down specimens for tension testing, low velocity impact testing, and residual bending strength testing. Uniaxial tensile tests per ASTM D3039 are conducted on the laminated facing to determine its tensile modulus of elasticity along the longitudinal direction. Low velocity impact tests using the DynaTup impact machine are conducted on the machined beam specimens per ASTM D2444 with varying hammer weights. After impact testing, the residual load carrying capacity of the sandwich beam specimens are determined using a four-point bending test. In this test, the ASTM C393 test method is followed. Mid-span deflections of the beams were again real-time measured using the LVDT.**

Keywords—Sandwich; fiber reinforced plastic; dynamic; flexural; impact.

1. INTRODUCTION

In the past decade, light-weight bridge deck systems made from Fiber Reinforced Polymer (FRP) composites have been developed and experimentally implemented in bridge structures. Composite sandwich construction is playing an increasingly important role in the design of structures because of its exceptionally high flexural stiffness-to-weight ratio. Typically, a sandwich composite consists of two thin, stiff and strong face sheets, separated by a thick, light and weaker core. The faces are adhesively bonded to the core to create a load transfer mechanism between the components. Historically, the advantages of the concept of using two co-operating faces separated by a distance go back to 1849 [1]. Since the late 1940's, the technology of sandwich laminates has progressed significantly and a comprehensive use of the advantages of sandwich laminates has been made. Commonly used face materials can be classified into two main groups: metallic and non-metallic materials. The former group includes steel, stainless steel and aluminum alloys. The later group includes plywood, cement and fiber composites. Light weight, high strength and excellent corrosion characteristics made fiber composites attractive face materials for manufacturers and engineers. Development of core materials has continued throughout the past sixty-five years in an effort to reduce the weight of the sandwich laminate. The cores used in sandwich construction can be divided into four main groups; corrugated, honeycomb, balsa wood and foams. Balsa wood was the first core material to be used in sandwich construction. The use of sandwich structures is growing very rapidly around the world. The need for light-weight structural elements with high stiffness for bridge applications and trucking industry increase the demand for sandwich construction technology made of composite materials.

A study about innovative alternative systems for FRP bridge decks and trucking industry was conducted by Hassan et al. [2]. Three-dimensional (3-D) fibers are used to connect the top and bottom GFRP layers using either weaving or injection technology. Addition of the through-thickness fibers increases the out of plane properties of the panel, delays delamination-type failures, allows low cost manufacturing and ensures full utilization of the panel strength. The study describes the fabrication process of 3-D FRP panels using the weaving technology. The panels consist of GFRP laminates and foam core sandwich where top and bottom skin GFRP layers are connected together with through-thickness fiber. The innovative core design provides an additional strength and stiffness over traditional foam core sandwich composites. Methods of assessment of the material characteristics in tension, shear and flexural are studied. Various means to test, design and optimize FRP sandwich panels are reviewed. The influence of the thickness of the panel, presence of filling material and density of 3-D fiber insertions are also discussed.

The feasibility of Glass Fiber Reinforced Polymer (GFRP) systems for low-profile bypass roadways was investigated by Rocca and Nanni [3]. An experimental program, including static and dynamic fatigue tests, is performed. The same type of specimens tested under static loading, are cyclically conditioned in order to determine its residual strength. The investigation focuses on the ultimate capacity and stiffness (compressive and flexural) of the sandwich structure, as well as its residual strength and rigidity after fatigue conditioning. The mechanical properties resulting from the experiments on virgin and fatigue-conditioned samples constitute the basis for the assessment and validation of the material system for the intended

application. A combined analytical and experimental study of dynamic characteristics of honeycomb composite sandwich structure in bridge systems is presented by Lestari and Qiao [4]. They claim that the procedure is especially practicable for estimating the beam transverse shear stiffness, which is primarily contributed by the core and is usually difficult to measure. The composite sandwich beams were made of E-glass fiber and polyester resins and the core consisted of the corrugated cells in a sinusoidal configuration. Based on the modeling of equivalent properties for the face laminates and core elements, analytical predictions of effective flexural and transverse shear stiffness properties of sandwich beams along the longitudinal and transverse to the sinusoidal core wave directions are first obtained. Using piezoelectric sensors, the dynamic response data are collected, and the dynamic characteristics of the sandwich structures are analyzed, from which the flexural and transverse shear stiffness properties are reduced.

Innovative fiber-reinforced polymer (FRP) composite highway bridge deck systems are gradually gaining acceptance in replacing damaged/deteriorated concrete and timber decks [5]. FRP bridge decks can be designed to meet the American Association of State Highway and Transportation Officials (AASHTO) HS-25 load requirements [5]. A finite-element analysis (FEA) that is able to consider the structural complexity of the entire bridge system and the material complexity of an FRP sandwich deck is presented in ref. [5]. The FEA is constructed using a two-step analysis approach. The first step is to analyze the global behavior of the entire bridge under the AASHTO HS-25 loading. The next step is to analyze the local behavior of the FRP deck with appropriate load and boundary conditions determined from the first step. For the latter, a layered FEA module is proposed to compute the internal stresses and deformations of the FRP sandwich deck.

Sandwich structures consisting of thermoplastic-based Fiber-Metal Laminate (FML) skins and aluminum foam core have been manufactured and tested under quasi-static and dynamic loading conditions by Villanueva [6]. The FML are based on unidirectional and woven glass fiber/polypropylene. Static tests are performed on beams of the hybrid systems using the three- point bend (3PB) test geometry. The low velocity impact response of these structures is evaluated using an instrumented dropping weight impact tower. Here, energy-absorbing mechanisms such as buckling and interfacial delamination in the FML skin, as well as indentation, crushing and densification in the aluminum foam have been observed to contribute to the excellent energy absorbing characteristics offered by these systems under low velocity impact loading conditions. The static and flexural fatigue characteristics of foam cored polymer composite sandwich beams are investigated by Shenoi et al. [7]. The skins of the beams are made from hybrid glass-aramid fibres set in epoxy resin and the core materials are linear and cross-linked polymer foams. The applied load in a ten-point configuration approximates a uniformly distributed load throughout the span of the beam which is simply supported at the ends. The testing frequencies are 0.33-0.91 Hz. Local regions of bond failure between face sheet and core are often observed when sandwich structures are exposed to low energy impacts [7]. Similarly, impact loads frequently result in delaminations within the face sheets. In the absence of any delaminations in the sandwich structure the buckling strain of the debonded region is shown to be the key parameter in assessing the structural integrity of a sandwich component in compression [7]. Effects of material properties and initial imperfections were examined in that study [7]. Analyses of the buckling of a delamination suggest that the effect of the core can be ignored. In contrast, the results showed that the core could not be ignored in the case of buckling of a debond nor could it be simulated in terms of simple boundary conditions. Influence of core properties on the failure of composite sandwich beams were studied by Daniel [8]. Composite sandwich structures were developed for the hydrofoil sail boat hull using biaxial carbon fabric/epoxy composite facing and agglomerated cork core [9]. Fiber metal laminates (FMLs) were used as skin on polypropylene honeycomb core to form a sandwich structure [10]. Impact response was measured by conducting a series of low-velocity impact test. It was found that the maximum impact load increased up to a threshold value at which it plateaus while the energy absorption in the structure increased with increasing impact energy. A study to compare the contribution of different core configurations to the accelerations exerted to the frame due to blast loading by numerical analysis was conducted by Athanasios et al. [11]. From the above extensive literature survey, studies on hybrid glass fiber and steel wire reinforced polymer composite deck are scarce. The purpose of this study is thus to investigate the flexural and dynamic behavior of the hybrid fiber reinforced polymer composite sandwich decks.

1.1 Fiber-Reinforce Plastic (FRP) and Hard-Wire Laminates Composite Beam

Fiber-reinforce plastic (FRP) laminates have received more and more attention due to their high specific strength, high specific stiffness and high durability over traditional metallic materials. In this study the flexural behaviors of the composite sandwich beams are determined and analyzed in both experimentally and numerically. The testing beam consists of rectangular end-grain balsa wood core wrapped circumferentially with two layers (+/-45° orientation) of E-glass fabric, then longitudinally on the top and bottom surfaces with two layers of the most dense Hardwire, then transverse to that one layer of medium density Hardwire. Lastly, the outer surfaces were wrapped with random glass mat, for an impact and water resistant outer layer of approximately 0.1 inch thickness. The entire assembly was vacuum-infused with vinyl ester resin containing Single Wall Carbon Nanotubes. In terms of the requirements of ASTM standard C393-00 [12], five specimens are tested using FORNEY universal testing machine. Three specimens are tested under 4-point bending load and the other two specimens are tested under 3-point bending load. These flexure tests (3- and 4-point bending) are used to determine the sandwich flexural stiffness, the core shear strength and shear modulus, or the facing bending strength based on the ASTM standard C393-00. Similar finite element model of the beam has been analyzed numerically using ANSYS. The mechanical properties of the skin and core material determined by experimental testing are applied to model. Similar loading and boundary conditions are considered, and the load-deflection of the model is determined and compared with that determined by experimental testing.

Fig. 1.   Five Beams with Strain Gauge

Table 1 Geometrical property of the specimens

Description	Length (in.)	Width (in.)	Thickness (in.)	Panel areal Weight (lb/ft^2)
Panel # 1	61.0	6.28	4.736	17.64
Panel # 2	61.0	6.33	4.719	17.56
Panel # 3	61.0	6.38	4.727	17.33
Panel # 4	61.0	6.42	4.74	17.25
Panel # 5	61.0	6.355	4.737	17.31

2. FLEXURAL TESTING

2.1 Test Fixtures and Instrumentation

Fig. 1 shows five beams with strain gauge and Fig. 2 shows the schematic view of the test fixtures and other instruments used in the 3- point bending test. Load is applied using a universal testing machine (FORNEY) from the bottom of the specimen. One fixture is used for 3-point bending test. The bottom fixture is supported by the FORNEY machine load plate and the upper fixture is restrained by the upper fixed frame of the machine. For measuring the deflection at the mid-span of the beam, a LVDT (displacement transducer) is attached at bottom (three-point bending) and top (four-point bending) of the mid-span of the beam and supported by the load plate of the machine. The LVDT is attached with a data acquisition unit (Cooper data chart 2000) which gives the instantaneous displacement of the beam. To determine local strain, the strain gauges are mounted at the top face, the side face, and the bottom face at the mid-span of each beam. A Yokogawa unit is used to measure the local strains of the beams.
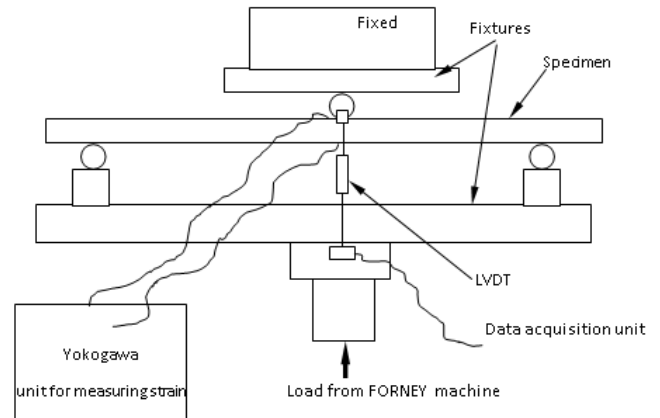

Fig. 2. Schematic view of test fixtures and other instruments for 3-point bending test

2.2. Description of Testing Procedure

The test specimen is placed above bottom fixture seated on the load cell of the FORNEY machine. The bottom fixture supports the specimen at the two ends of the specimen and load is applied at a constant rate at the two points on the bottom surface. For three-point bending (Fig. 3), the top fixture supports the beam at the mid-span. As the load is increased, deflection at the center increases. Deflection is measured by means of Linear Voltage Differential Transformer (LVDT), located above the midpoint of the specimen. The LVDT is connected to a data acquisition unit which gives the instantaneous displacement of the beam. The strain gauges are placed at different locations (middle top, middle bottom, and middle side face) of the beam to measure the local strain of the beam. Load versus deflection plots are generated and analyzed to find the flexural properties of the beams.

Fig. 3.   Side view of specimen, strain gauge wire and LVDT attachment for a 3-point bending test

2.3. Testing Results

2.3.1   Three-Point Bending Test Results

Three-point bending test loading configuration is shown in Fig. 4. Two specimens were tested under three-point bending and the load versus deflection graphs for those tests are shown

in Fig.s 5 and 6. The first part of the graph in Fig. 5 is linear and the 2nd part is non-linear and the third part is again linear. During the test small wooden pieces were used to increase the space between the specimens and the bottom fixture. During the test the wooded pieces deformed and the load-deflection graph fluctuated (Fig. 5). The 2nd test was conducted using metal pieces (the roller) and the graph looks very fine in the linear portion (Fig. 6).
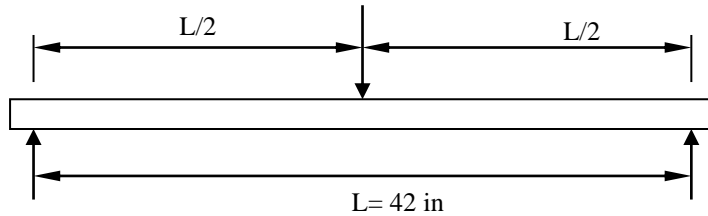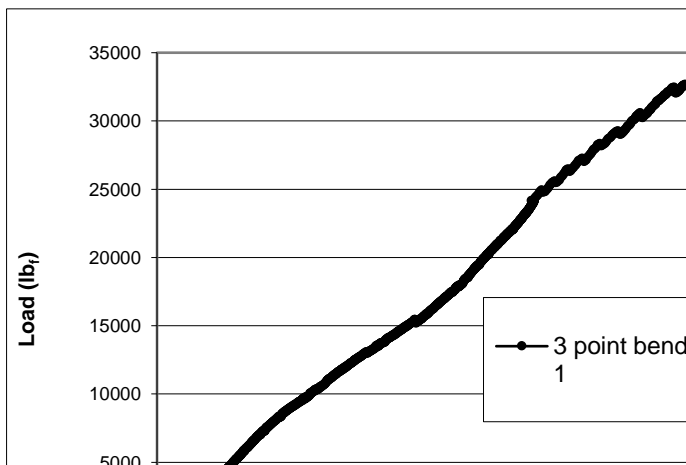

Fig. 4. A 3-point bending load

Fig. 5. Load versus deflection at the middle of the beam for specimen 1
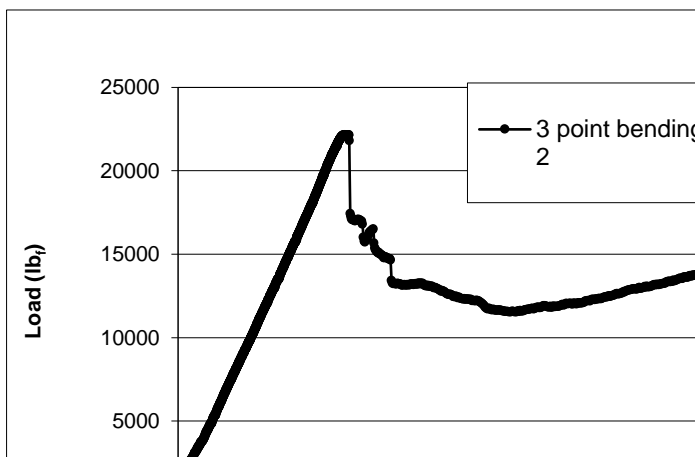
Fig. 10: Load versus deflection at the middle of the beam for specimen 2

For three-point bending test, core shear strength of the beam specimens was calculated using (1). Facing bending strength, σ of the beam specimens was calculated using the following equation:

$$\sigma = \frac{PL}{2t(d+c)b} \qquad (1)$$

and the laminate stiffness, D was found from the following equation [13]:

$$\Delta_{total} = \underbrace{\frac{PL^3}{48D}}_{bending} + \underbrace{\frac{PL}{4U}}_{shear} \qquad (2)$$

where
P = failure load, N;
d = beam depth, m.;
b = beam width, m.;
c = core thickness, m;
t = thickness of facing, m;
L = Support span, m.

The various properties of the specimens were calculated using the data of the load-deflection graphs and the results are given in Table 3.

2.4 Comparison of Measured Strain and Calculated Strain at Mid-Span

During the experimental test, strain gauges were mounted at the mid-span on the top and bottom surfaces to obtain local strain. Fig.s 6 present the moment distribution in the 3- point bending tests. In order to validate if the Euler beam theory was applicable or not, a theoretical analysis was conducted to compare with the experimental results. From flexural bending of a Euler beam [13], we have the following relation between the strain and bending moment:

$$\varepsilon = \frac{My}{EI} \qquad (3)$$

where: ε = normal strain at a point with a distance y from the neutral axis; M = bending moment, lb$_f$-in; EI = bending stiffness, lb$_f$ /in^2; y = distance from neutral axis to desired point.
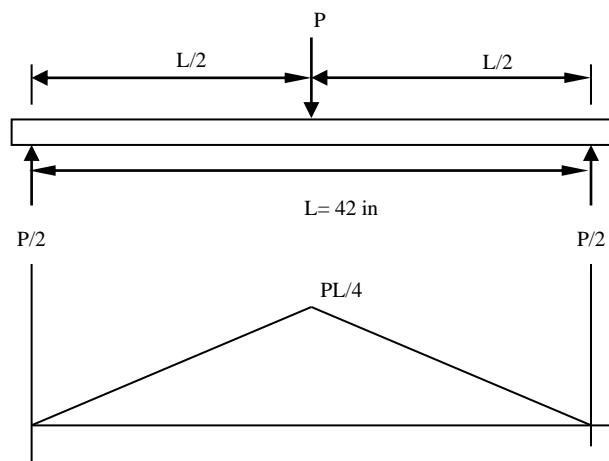

Fig. 6. Bending moment diagram for 3-point bending load

Table 2: Various properties of the beam calculated from 3-point bending

Specimen	failure load P (lb)	Facing bending strength (psi)	Core Shear strength (psi)	Bending stiffness D ($\times 10^6$ lb-in^2) using Eq. (2)	Bending stiffness EI ($\times 10^6$ lb-in^2) using Eq.(3)	Facing modulus ($\times 10^6$ psi) using Eq. (3)	Facing modulus ($\times 10^6$ psi) using Eq. (2)
1	24,170	25,478	434.95	40.12	43.81	2.01	1.84
2	22,150	23,348	398.60	58.40	48.50	2.22	2.67

The comparison of maximum strain from theoretical and experimental analysis on the bottom surface at the mid-span for the 3-point bending is given in Table 6. For three-point bending tests, the theoretical estimation is close to the strain gage measurement.

Table 3: Comparison of maximum strain between theoretical and experimental analysis for 3-point bending tests

Test-3 point bending	Theoretical strain	Experimental stain	Deviation (%)
Specimen 1	0.013706207	0.0145	5.47
Specimen 2	0.011344763	0.01346	15.71

3. LOW VELOCITY IMPACT TESTING

Composite sandwich structures have been recognized as having higher bending strength, lower weight, and higher durability. For composite sandwich structures, they usually contain laminated composite skins. It is well known that laminated composites are vulnerable to impact damages, in particular to low velocity impact induced damages. After a low velocity impact, the residual strength or stiffness of the laminate can be reduced significantly. What make things even worse is that low velocity impact damages usually avoid visual detection. Most of the time, only a small indentation can be identified on the impacted surface after a low velocity impact; however, significant delamination, matrix cracking, fiber breaking, and fiber/matrix interfacial debonding may have been produced inside the specimen and on the back surface. A low velocity impact is not uncommon. A dropping of a tool during a routine inspection characterizes a low velocity impact. For the sandwich deck, it cannot be avoided that some low velocity impacts may occur during transportation and installation, or during paving the asphalt or concrete wearing course. Therefore, it would be beneficial to have a prior knowledge of the impact resistance and residual strength of the selected composite deck. Once this information is known, safety measures can be taken, for instance to increase the safety factor and be more cautious during construction so that a safe and reliable composite deck can serve the anticipated traffic loads.

3.1 Description of Impact Tester

The DynaTup Model 8250HV impact test machine (Fig. 7) was used for the low velocity impact testing. This drop-weight tester combines gravity with pneumatic assistance to cover a wide range of impact velocities up to 14m/s. With the combination of available weights that alter the hammer weight, impact energy up to 4,450 J can be achieved. An environmental conditioning chamber is integrated with the equipment. The temperature range is controlled with an electronic thermostatic controller from –58 °F to +347 °F. The clamping fixture, which simulates a rigid clamping with a force of 160 lbs is located within this environmental chamber, ensuring that specimens are tested at the desired temperature. Communication and data acquisition with the impact test machine is via a computer integrated control and data acquisition system.

Fig. 7. DynaTup 8250 HV Impact Machine

3.2 Specimen Preparation and Impact Test

Due to test chamber height limitation of the DynaTup impact test machine, specimens of sizes about $2 \times 2.36 \times 10$ in. were cut from the overhanging portion of the full-scale beam tested previously. This portion was not loaded in the previous test and thus was treated as virgin. The beams were cut at the middle depth. As a result, the specimens had only one skin and a core with only half thickness, as schematically shown in Fig. 8.
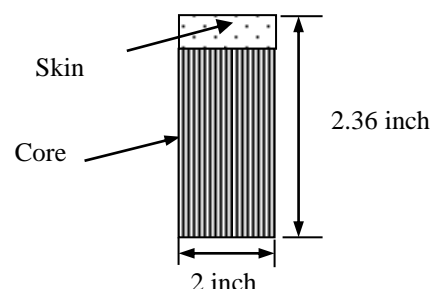

Fig. 8. Cross section of impact test specimen

Once the specimens were prepared, they were impact tested. The laminated skin was the front surface that was directly impacted and the half-core was used as a support to the skin. It is believed that the impact damage to this type of specimens would be larger than the actual specimens, which have the whole thickness of the core and the bottom skin to provide a stronger support to the front skin. Due to the limitation of the available virgin portions from the previous full-scale beam tests, only two specimens were prepared and tested for each hammer weight. In this study, the impact velocity was fixed at 12.56 ft/s and three hammer weights were used: 25 lb, 50 lb, and 75 lb. The test temperature was about 60 °F. The load-time and energy-time curves for each specimen are shown in Fig.s 9-14.

3.3   Impact Test Results and Discussions

In Fig.s 9-14, the red curve represents the load-time history and the black curve represents the energy-time history. The load-time history has two regions, a region of damage initiation and a region of damage propagation. As the load increases during the damage initiation phase, elastic strain energy is accumulated in the specimen and no gross failure takes place; but failure mechanisms on a micro scale such as micro-buckling of the fibers on the compression zone or de-bonding at the fiber-matrix interface are possible. When a critical load (peak load) is reached at the end of the initiation phase, the composite beam specimen may fail either by a tensile or a shear depending on the relative values of the tensile and interlaminar shear strength. From this point the fracture propagates either in a catastrophic brittle manner or in a progressive manner continuing to absorb energy- at smaller loads. In the impact tests, it was observed that the specimens failed by an indentation at the front skin, delamination of the skin, debonding of the skin from the core, and shear of the core; see Fig.s 15-17.

The peak load, the initiation energy and the propagation energy for different impact tests are summarized in Table 8. It is found that, in general, the initiation energy decreases and the propagation energy increases as the hammer weight increases. This suggests that, as the hammer weight increases, the damage are extended to a larger area. More materials are involved and affected by damage with a higher hammer weight. To the contrary, the damage by a lower weight hammer is localized and the effect on the load carrying capacity is also limited. Because of this, it is expected the effect of the impact on the residual load carrying capacity will be different depending on the hammer weight. This will be examined in the next section.

Table 8: The peak load, initiation and propagation energy for different impact tests

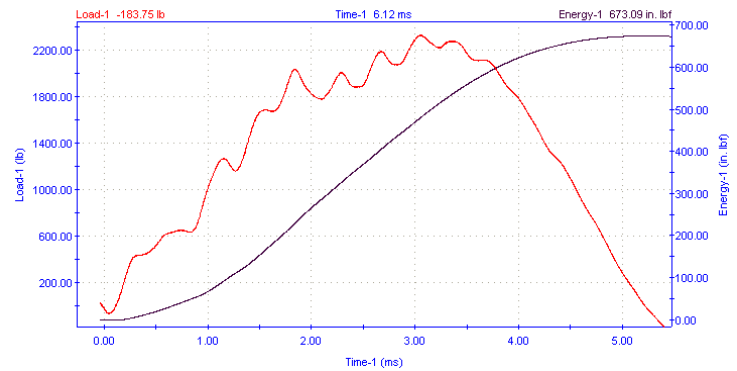| Specimen (hammer weight and specimen #)	Peak load (lb$_f$)	Initiation energy (lb-in)	Propagation energy (lb-in)	Ratio of propagation to initiation energy (lb-in)
25 lb #1	2300	470	200	0.43
25 lb #2	3300	670	40	0.06
50 lb #1	3870	1200	340	0.28
50 lb #2	3800	700	820	1.17
75 lb #1	4025	550	2170	3.94
75 lb #2	4300	800	1880	2.35

Fig. 9.   Load and energy distribution after impact (impact mass = 25 lb, velocity =12.53 ft/s, specimen 1)
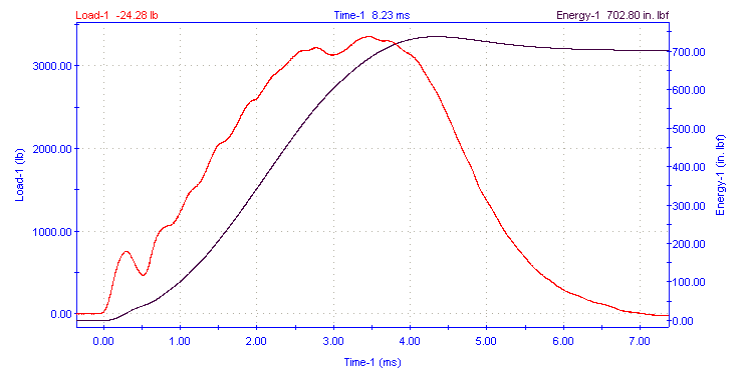

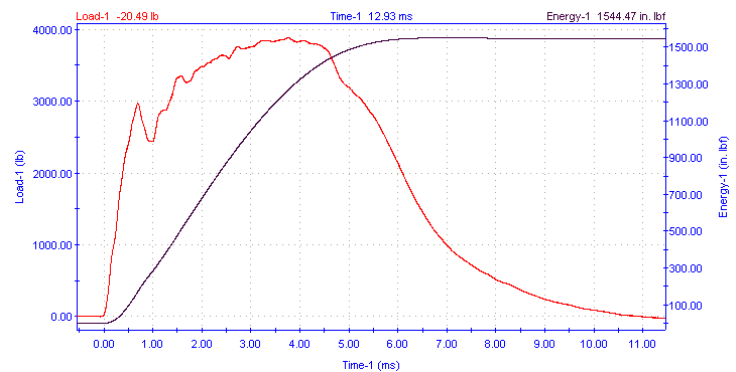Fig. 10. Load and energy distribution after impact (impact mass = 25 lb, velocity =12.53 ft/s, specimen 2)

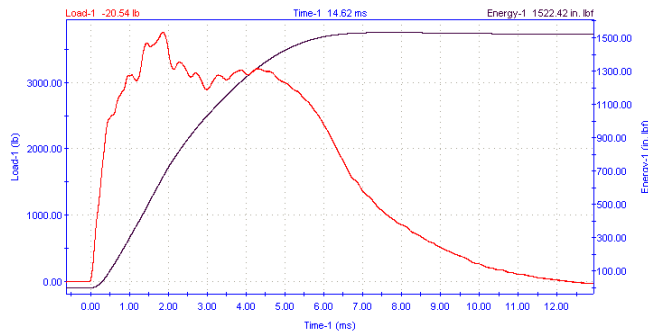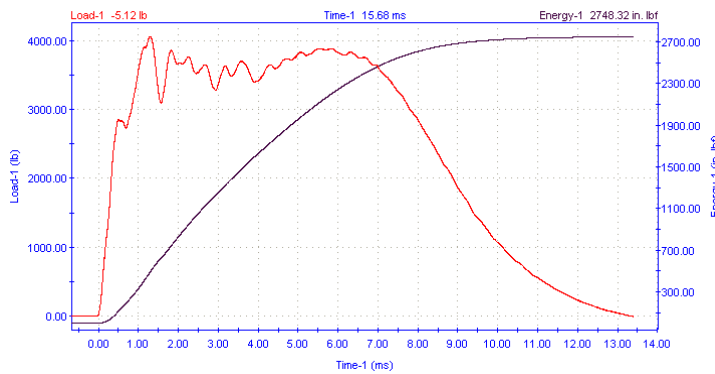Fig. 11. Load and energy distribution after impact (impact mass = 50 lb, velocity =12.56 ft/s, specimen 1)

Fig. 12. Load and energy distribution after impact (impact mass = 50 lb, velocity =12.56 ft/s, specimen 2)

Fig. 13. Load and energy distribution after impact (impact mass = 75 lb, velocity =12.56 ft/s, specimen 1)
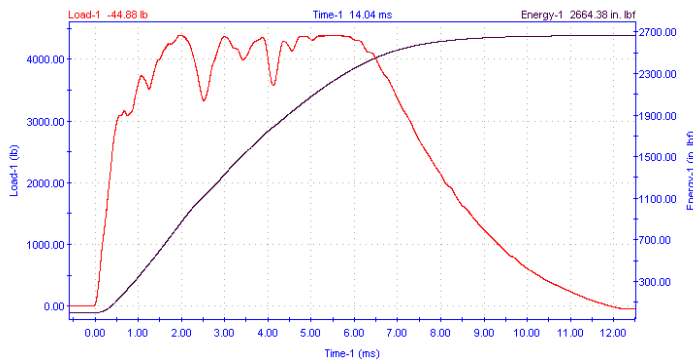

Fig. 14. Load and energy distribution after impact (impact mass = 75 lb, velocity =12.56 ft/s, specimen 2)

Fig. 15. Indentation

Fig. 16. Interfacial debonding and core shear failure

Fig. 17. Skin delamination

4. RESIDUAL BENDING STRENGTH USING 4-POINT BENDING TEST

After the impact test, the specimens were tested using a 4-point bending load to obtain the residual flexural properties of the beam. The details of the test are given in the next section.

4.1 Specimens Preparation

After the impact test, each specimen was glued with another untested specimen of the same size to recover the two-skin sandwich beam specimen tested previously. The approximate specimen's size is $2 \times 4.75 \times 10$ in. The loading configuration for the 4-point bending test is shown in Fig. 18. Seven specimens were tested under the 4-point bending load (six impact damaged specimens and one undamaged control specimen). The impacted skin was in the compressive zone.
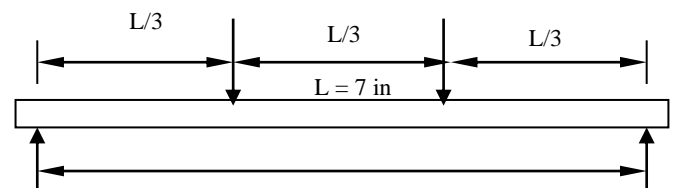

Fig. 18. A 4-point bending load
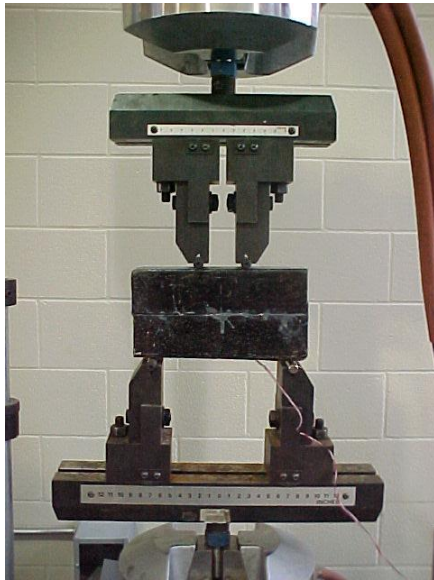
4.2 Description of Test Procedure

Fig. 19. A specimen under four-point bending test

The test was conducted using the MTS 810 machine. The test specimen was placed onto the bottom fixture seated on the load cell of the MTS machine. The bottom fixture supported the specimen at the two ends of the specimen and load was applied at a constant rate at the two points on the bottom surface. As the load was increased, deflection at the center increased. Deflection was measured by means of the same LVDT, located above the midpoint of the specimen. The LVDT was connected to a data acquisition unit which gave the instantaneous displacement of the beam. The strain gauges were placed at the bottom mid-span of the beam to measure the local strain of the beam. Load versus deflection plots were generated and analyzed to find the flexural properties of the beams. Fig. 19 shows a specimen under the four-point bending test. The load versus deflection graphs are shown in Fig.s 20-26.
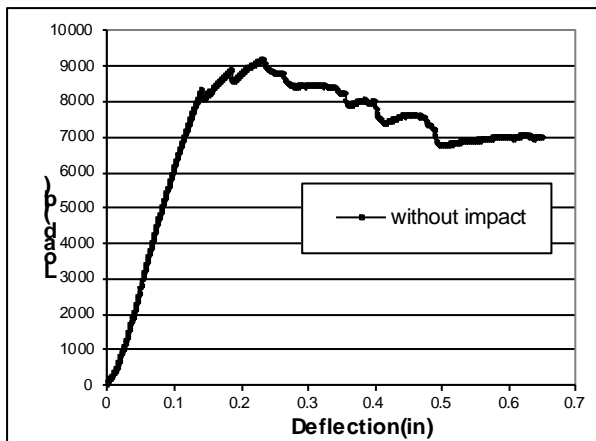

Fig. 20. Load versus deflection at the middle of the beam for specimen without impact
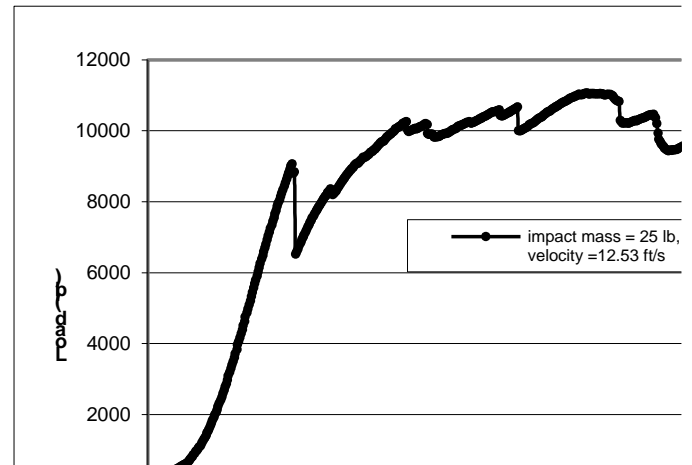

Fig. 21. Load versus deflection at the middle of the beam after impact (impact mass =25 lb, velocity = 12.53ft/s, specimen -1)
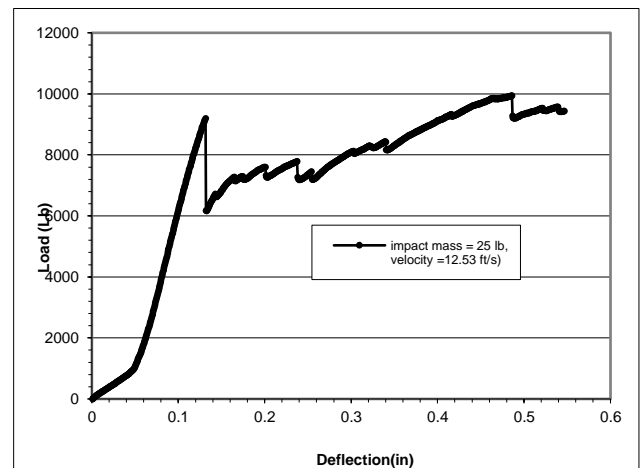

Fig. 22. Load versus deflection at the middle of the beam after impact (impact mass =25lb, velocity = 12.53ft/s, specimen-2)
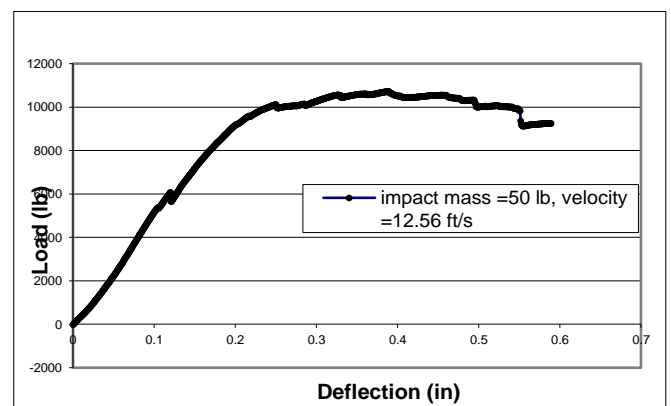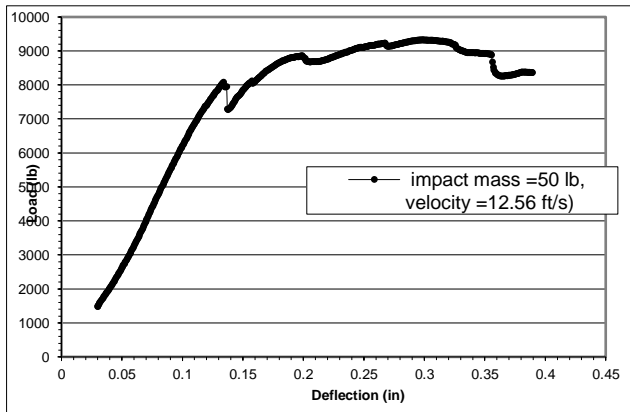

Fig. 23. Load versus deflection at the middle of the beam after impact (impact mass =50 lb, velocity = 12.56 ft/s, specimen-1)

Published by :

http://www.ijert.org

International Journal of Engineering Research & Technology (IJERT)
ISSN: 2278-0181
Vol. 9 Issue 06, June-2020

Load versus deflection at the middle of the beam after impact (impact mass =50 lb, velocity = 12.56 ft/s, specimen-2)

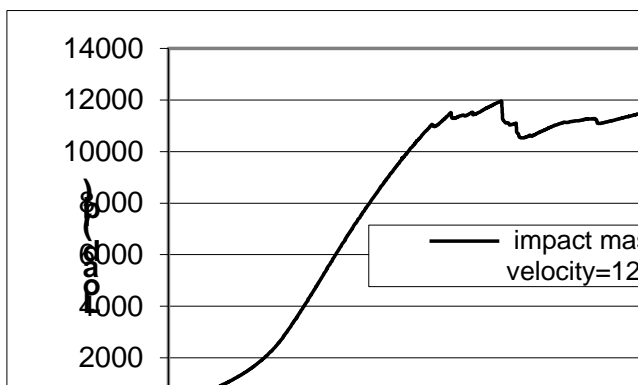Fig. 24. Load versus deflection at the middle of the beam after impact (impact mass =75 lb, velocity = 12.56 ft/s, specimen -1)
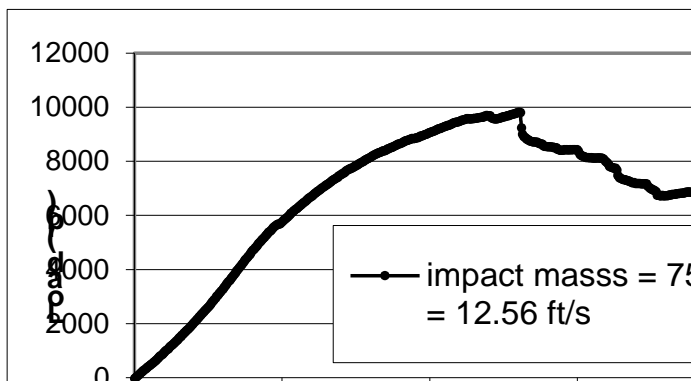

Fig. 25. Load versus deflection at the middle of the beam after impact (impact mass =75 lb, velocity = 12.56 ft/s, specimen-2)

From the load-deflection graphs, various properties of the beams were calculated. The maximum loads were used to calculate the core shear strength and facing bending strength of the specimens. Equations (1), (2) and (4) were used to calculate the core shear strength, facing bending strength and bending stiffness respectively. It is noted that the calculated results are meaningful only for comparisons. They do not represent the actual strength and stiffness. The reason for this is that the specimens are considered to be deep and short beams. The equations from ASTM C393 are not suitable for

calculating the actual strength and stiffness of such types of short and deep beams. Also, the full-scale beams had a transverse reinforcement because they were fully wrapped by the FRP. However, the scaled-down specimens for the impact tests were machined from the full-scale beams and the transverse reinforcement was removed. This inevitably resulted in lower strength and stiffness. The failure load and the various calculated results are summarized in Table 9.

Table 9: Various properties of the specimens calculated from the 4-point bending test

Specimen	Core Shear strength (psi)	Facing bending strength (psi)	Bending stiffness EI (lb-in^2)	% reduction in bending stiffness	Facing modulus E (psi)	% reduction in facing modulus
Control	529	3442	389779	0	57951	0
25 lb #1	523	3405	277083	-28.9	36381	-37.2
25 lb #2	577	3754	285334	-26.7	37276	-35.6
50 lb #1	482	3134	265881	-31.7	34725	-40.0
50 lb #2	591	3844	241776	-37.9	35375	-38.9
75 lb #1	578	3763	230504	-40.8	26985	-53.4
75 lb #2	502	3268	234431	-39.8	30069	-48.1

Compared with the control specimen, it is found that the core shear strength and the facing bending strength are generally not affected by the impact load. This may be explained by the failure mode of the bending specimens. The specimens failed by local buckling of the skin and/or shear failure of the core at or near the rollers of the support span, which are far away from the mid-span (the point directly under impact). Fig. 27 shows a failure mode of such a specimen. It failed by core shear and transverse shear. The reason for transverse shear failure is that the beam is considered to be a deep and short beam. Transverse shear failure predominates in short beams. No skin tensile failure was observed. Therefore, the damage by the impact cannot take effect on reducing the bending strength before such type of premature failures occurs. The bending stiffness and the facing modulus are considerably affected by the impact damage. These properties decrease as the impact load increases. This suggests that during the structural design of the composite deck, the reduction in stiffness due to impact needs to be considered.

Fig. 26. Core shear failure and transverse shear failure

4. CONCLUSIONS

Four types of tests were conducted on the selected composite sandwich beams. One was a flexure test on the as-received full-scale beams. Both three-point bending and four-point bending test were conducted. Various properties of the sandwich beams were calculated. The second type of tests was a uniaxial tension test. The modulus of elasticity of the laminated composite facing was determined. The third type of tests was a low velocity impact tests. One velocity and three hammer weights were used. The last type of tests was again a four-point bending test on the impact damaged specimens. All the tests were conducted per pertinent ASTM standards. A finite element analysis was also conducted to validate the material properties estimated. The findings from this study are as follows:

The full-scale sandwich beams have all failed in the compression zone by local buckling of the top face and shear of the core. The bottom skin does not exhibit any type of premature failure or distress. No debonding failure in the tension zone is observed in any of the tested beams.

Four-point bending test and three-point bending test yield different strength and stiffness. In general, three-point bending test gives lower strength and stiffness.

The facing modulus of elasticity cannot be accurately determined using the bending test results. Uniaxial tensile tests must be used. In general, the uniaxial tensile test yields higher modulus of elasticity than that obtained from bending tests.

There is a considerable difference between the theoretical strain based on Euler beam theory and the measured strain using strain gages. The Euler beam theory cannot be used to describe the behavior of the sandwich beam. A higher order laminated beam theory with a consideration of the transverse shear must be used.

A reasonable tendency in the load-deflection curves is found between the results from the three-point bending tests and those obtained by the company. With the same applied load, the deflection from this study is slightly higher than that by the company possibly due to the distributed load from the tire used by the company. The propagation energy increases as the impact load increases, suggesting that more materials are involved in damage during the low velocity impact.

The effect of the low velocity impact on the residual bending strength is minimal; a considerable reduction is observed for the residual bending stiffness. The skin can be reasonably treated as a quasi-isotropic laminate. The material properties used in the finite element modeling, which were estimated from the test results and literatures, lead to acceptable results.

ACKNOWLEDGEMENT

REFERENCES

[1] Zenkert, D., "The Hand Book of Sandwich Construction," Chameleon Press Ltd, London, UK, 442, 1997.

[2] Hassan, T., Reis, E.M., and Rizkalla, S.H., " Innovative 3-D FRP Sandwich Panels for Bridge Decks" *Proceedings of the Fifth Alexandria International Conference on Structural and Geotechnical Engineering*, Alexandria, Egypt, Dec. 2003.

[3] Rocca S.V. and Nanni A. "Mechanical Characterization of Sandwich Structure Comprised of Glass Fiber Reinforced Core: Part 1," Composite in Construction 2005-Third International Conference, Lyon, France, July 11-13, 2005.

[4] Lestari W. and Qiao P., "Dynamic Characteristics and Effective Stiffness Properties of Honeycomb Composite Sandwich Structures for Highway Bridge Applications," J. of Composite for Construction, Volume 10, Issue 2, pp. 148-160, 2006.

[5] 5. *Bin M., Hwai-Chung W., An Y., Kraig W., Gongkang F., Ronald F.G., and Dong-Woo K. "FEA of Complex Bridge System with FRP Composite Deck," J. Composite for Construction., Volume 10, Issue 1, pp. 79-86, 2006.*

[6] Villanueva G. R. "Failure Mechanisms in FML Reinforced Aluminum Foam Sandwich Structures," Proceedings of the Conference of Society for the Advancement of Material and Process Engineering, Long Beach, CA, April 30-May 4, 2006.

[7] Shenoi R.A., Clark S.D. and Allen H.G. "Fatigue Behaviour of Polymer Composite Sandwich Beams," Journal of Composite Material, Vol. 29, No. 18, 2423-2445, 1995.

[8] Issac M. Daniel (2009). Influence of core properties on the failure of composite sandwich beams, *Journal of Mechanics of Material and Structure,* **4**: 1271-1286.

[9] C. Y. Tan and Hazizan Md. Akil (2012). Impact response of fiber metal laminate sandwich composite structure with polypropylene honeycomb core, Composites Part B: Engineering, 2012, Vol **43**, Issue 3, pp. 1433-1438.

[10] Athanasios Kotzakolios, Dimitrios Vlachos, Christos Derdas and Vassilis Kostopoulos (2014). On the blast response of sandwich aerospace composites, *Int. J. of Computer Aided Engineering and Technology*, Vol.**6**, No.4, pp.383 – 403.

[11] ASTM C 393-00, Standard Test Method for flexural properties of Sandwich Construction.

[12] R.C. Hibbeler (2003). *Mechanics of Material*, sixth edition, 2003, pp. 588.